LANGMUIR

pubs.acs.org/Langmuir Article

Computational Investigation of Antifouling Property of Polyacrylamide Brushes

Yonglan Liu,[#] Dong Zhang,[#] Baiping Ren, Xiong Gong, Aristo Liu, Yung Chang, Yi He, and Jie Zheng[*]

Cite This: *Langmuir* 2020, 36, 2757−2766 Read Online

ACCESS | Metrics & More | Article Recommendations | Supporting Information

ABSTRACT: Antifouling materials and coatings have broad fundamental and practical applications. Strong hydration at polymer surfaces has been proven to be responsible for their antifouling property, but molecular details of interfacial water behaviors and their functional roles in protein resistance remain elusive. Here, we computationally studied the packing structure, surface hydration, and protein resistance of four poly(*N*-hydroxyalkyl acrylamide) (PAMs) brushes with different carbon spacer lengths (CSLs) using a combination of molecular mechanics (MM), Monte Carlo (MC), and molecular dynamics (MD) simulations. The packing structure of different PAM brushes were first determined and served as a structural basis for further exploring the CSL-dependent dynamics and structure of water molecules on PAM brushes and their surface resistance ability to lysozyme protein. Upon determining an optimal packing structure of PAMs by MM and optimal protein orientation on PAMs by MC, MD simulations further revealed that poly(*N*-hydroxymethyl acrylamide) (pHMAA), poly(*N*-(2-hydroxyethyl)acrylamide) (pHEAA), and poly(*N*-(3-hydroxypropyl)acrylamide) (pHPAA) brushes with shorter CSLs = 1−3 possessed a much stronger binding ability to more water molecules than a poly(*N*-(5-hydroxypentyl)acrylamide) (pHPenAA) brush with CSL = 5. Consequently, CSL-induced strong surface hydration on pHMAA, pHEAA, and pHPAA brushes led to high surface resistance to lysozyme adsorption, in sharp contrast to lysozyme adsorption on the pHPenAA brush. Computational studies confirmed the experimental results of surface wettability and protein adsorption from surface plasmon resonance, contact angle, and sum frequency generation vibrational spectroscopy, highlighting that small structural variation of CSLs can greatly impact surface hydration and antifouling characteristics of antifouling surfaces, which may provide structural-based design guidelines for new and effective antifouling materials and surfaces.

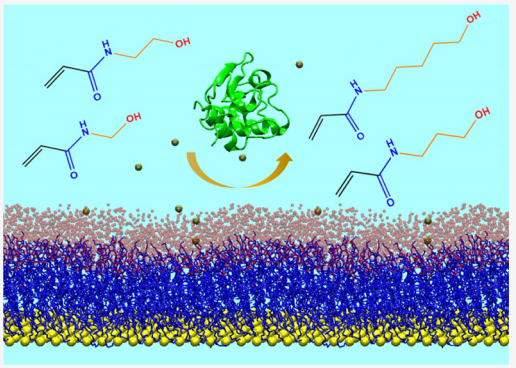

INTRODUCTION

Biofouling is a long-standing, global problem today,[1] which arises from the nonspecific interactions between artificial surfaces and foulants (e.g., proteins, cells, and bacteria) and significantly impedes a wide variety of applications, including marine coatings/hulls, biosensors, water pipes, filtration membrane, and biomedical engineering (e.g., sutures, surgical products, and wound healing dressings).[2−11] Significant efforts and progress have been made to develop many antifouling materials and surfaces, including hydrophilic polymers [e.g., poly(ethylene glycol) (PEG),[12,13] poly(acrylamide),[14] poly-(saccharides),[15] polypeptoids,[16] and poly(hydroxyethyl meth-acrylate),[17] zwitterionic polymers [e.g., poly(sulfobetaine methacrylate),[18−24] poly(carboxybetaine methacrylate),[24,25] poly(carboxybetaine acrylamide),[26,27] and poly(3-(1-(4-vinyl-benzyl)-1*H*-imidazol-3-ium-3-yl)propane-1-sulfonate)[28,29]], and self-assembling monolayers (SAMs) terminated with different functional groups (e.g., OEG,[30,31] −COOH,[32] and −PC[33,34]). All of antifouling materials/surfaces, despite different chemical structures and chemistry, share a similar strong binding ability to water molecules, creating a tightly bound water layer to reduce the interactions between the foulant and the surfaces.[35−39] Hydrophilic and zwitterionic materials/coatings generate strong surface hydration via hydrogen bonding and ionic solvation, respectively. Under the optimal conditions, the above-mentioned antifouling surfaces can achieve superior fouling performance even in complex media, as evidenced by low-protein adsorption (0.3−5 ng/cm^2 in the blood plasma and serum media), cell adhesion, and bacterial attachment.

In parallel to massive experimental studies of antifouling materials in terms of their materials synthesis and characterization, surface coating strategies, in vitro and in vivo tests at macroscopic length and timescales, molecular simulations have been used to investigate the structural, dynamical, and interfacial properties of antifouling materials at a molecular

Received: January 19, 2020
Revised: February 23, 2020
Published: March 2, 2020

https://dx.doi.org/10.1021/acs.langmuir.0c00165
Langmuir 2020, 36, 2757−2766

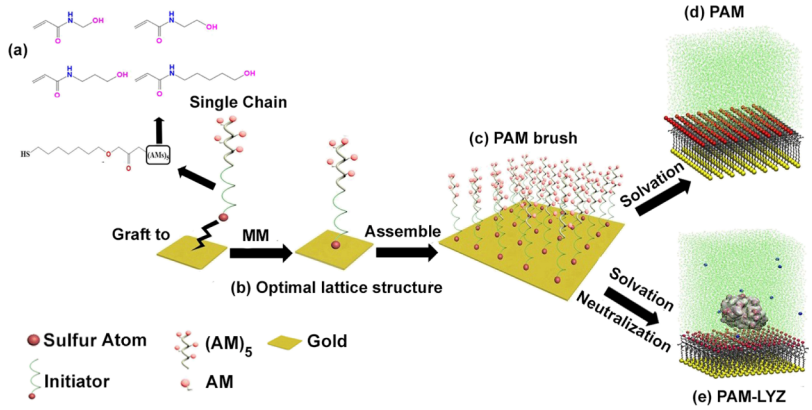

Figure 1. Schematic illustration of the modeling process of PAM brushes in the absence and presence of lysozyme.

level. Early molecular simulations mainly focused on the interfacial water behaviors on short SAMs with different end-groups,[12,40,41] partially because of the simplicity of simulation systems, the accessibility of experimental data, and less computational cost.[30,35,42] It was found that in contrast to CH_3-terminated SAMs, PEG-, PC-, and OH-terminated SAMs can form strong interactions with interfacial water,[41,43−46] suggesting the importance of surface hydration responsible for antifouling behavior. To expand the surface hydration hypothesis to long-chain polymer-grafted surfaces, subsequent computational simulations were applied to much more complex polymer-grafted surfaces in the absence and presence of a foulant or a protein. Different from SAM surfaces formed by short and rigid chains with little or neglectable conformational changes, polymer-grafted surfaces formed by long chain polymers usually undergo large conformational changes, which are affected by grafting density, chain length, and end-group hydrophobicity of grafting polymers. A number of molecular dynamics (MD) simulations have examined the degree of conformational transitions for grafting polymers as a function of grafting density, chain length, and end-group hydrophobicity without a foulant, as well as a structure−property relationship between the structural characteristics of grafting polymers and the dynamics of the hydration layer at polymer−water interfaces.[47−50] It was reported that antifouling efficacy of polymer-grafted surfaces increases with a longer chain length, higher grafting density, or helical-like structure, indicating that interfacial hydration by controlling the structure of grafted polymer chains is a key contribution to antifouling efficacy. Furthermore, more advanced steered MD (SMD) simulations were proposed and developed to study the adsorption of a foulant or protein on different polymer-grafted surfaces. Liu et al.[51] studied molecular structure and water diffusion at PVDF-*g*-DMAPS membranes using both conventional MD and SMD simulations. They observed the existence of the hydration layer at the water−membrane interface, where the enhanced HB strength and electrostatic repulsion dominate the antifouling capability. Leng and co-workers[52,53] investigated the surface hydration and antifouling behavior of PEG- and poly(sulfobetaine)-grafted membranes when a alginate foulant approached both membranes using SMD simulations, which revealed strong repulsive forces between the foulant and both membranes because of the compression of this hydration layer, regardless of surface chemistry and grafting density, confirming good antifouling properties.

All of the above-mentioned simulations of antifouling materials with and without foulants highlight the importance of surface hydration for antifouling properties of materials and surfaces. However, these simulation models were setup to mimic polymer-grafted brush on a gold chip using typical sulfur−gold (S−Au) bonds, and they did not consider the optimal lattice structure of polymer chains. Instead these models often assume the conventional $\sqrt{3} \times \sqrt{3}R30°$ lattice structure of the polymer chain with a chain−chain separation distance of 4.95 Å. Our previous computational work[12] on the structure of PC-terminated and OEG-terminated SAMs has demonstrated that different from a $\sqrt{3} \times \sqrt{3}R30°$ lattice structure of OEG-SAM, PC-SAMs adopts a $\sqrt{7} \times \sqrt{7}R19°$ lattice structure because of the size and polarity of head groups.

Herein, we employed molecular simulations with explicit water to computationally study the packing lattice structure, surface hydration, and protein interaction of poly(*N*-hydroxyalkyl acrylamides) (PAMs) brushes with different carbon spacer lengths (CSLs), that is, poly(*N*-hydroxymethyl acrylamide) (pHMAA) (CSL = 1), poly(*N*-(2-hydroxyethyl)-acrylamide) (pHEAA) (CSL = 2), poly(*N*-(3-hydroxypropyl)-acrylamide) (pHPAA) (CSL = 3), and poly(*N*-(5-hydroxypentyl)acrylamide) (pHPenAA) (CSL = 5). *N*-Hydroxymethyl acrylamide (HMAA), *N*-(2-hydroxyethyl)-acrylamide (HEAA), *N*-(3-hydroxypropyl)acrylamide (HPAA), and *N*-(5-hydroxypentyl)acrylamide (HPenAA) monomers contained one, two, three, and five methylene groups between hydroxyl and amide groups, while the other groups in polymer backbones were the same as each other. We first systematically explored and determined optimal lattice structures of different PAMs on the Au(111) substrate at the lowest-energy state from a large energy landscape. Because of the presence of the relatively large head groups (e.g., secondary amide, hydroxymethyl, hydroxyethyl, hydroxypropyl, and hydroxypentyl groups) of PAMs, all PAMs accommodated the much larger lattice structures than a conventional $\sqrt{3} \times \sqrt{3}R30°$ lattice structure. Based on optimal lattice structures of PAMs, CSL-induced surface hydration and protein interaction of PAMs were further explored and compared to reveal their brush structure−surface hydration−protein resistance relationship. Collective simulation data from radius distribution functions (RDFs), coordination number, self-diffusion, and mean residence time of interfacial water molecules revealed that pHMAA, pHEAA, and pHPAA (CSL = 1, 2, and 3) induced a stronger and more stable interaction with surrounding water molecules than pHPenAA (CSL = 5),

https://dx.doi.org/10.1021/acs.langmuir.0c00165
Langmuir 2020, 36, 2757−2766

Table 1. Geometric Parameters of 28 Unit Cells for a Single PAM Chain

lattice name	a (Å)	b (Å)	γ (deg)	area (Å^2)	lattice name	a (Å)	b (Å)	γ (deg)	area (Å^2)
4a	5.768	4.995	90	28.8	9b	8.652	7.630	79.1	64.8
4b	5.768	5.768	60	28.8	10a	9.990	10.398	43.9	72.0
5	7.630	4.995	70.9	36.0	10b	10.398	7.630	65.2	72.0
6a	8.652	4.995	90	43.2	10c	7.630	9.990	70.9	72.0
6b	9.990	4.995	60	43.2	10d	14.420	4.995	90	72.0
6c	8.652	5.768	60	43.2	10e	14.420	5.768	60	72.0
6d	5.768	7.630	79.1	43.2	10f	15.260	4.995	70.9	72.0
7	7.630	7.630	60	50.4	11a	12.570	7.630	55.8	79.3
8a	11.536	4.995	90	57.6	11b	7.630	10.398	90	79.3
8b	11.536	5.768	60	57.6	12a	11.360	8.652	61.6	86.4
8c	10.398	5.768	73.9	57.6	12b	8.652	10.398	73.9	86.4
8d	9.990	7.630	49.1	57.6	12c	14.980	7.630	48.2	86.4
8e	9.990	5.768	90	57.6	12d	11.360	7.630	85.6	86.4
9a	8.652	8.652	60	64.8	12e	8.652	9.990	90	86.4

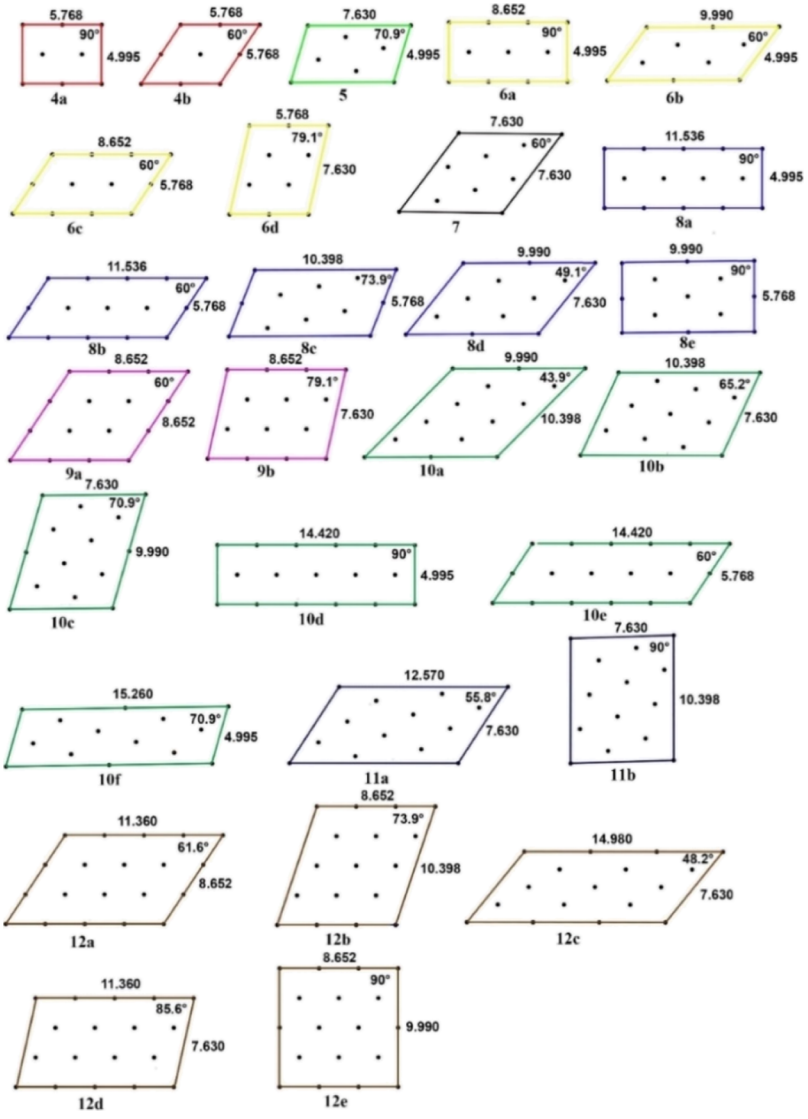

Figure 2. Schematic of unit cells to accommodate a single PAM chain. All of unit cells are defined by their lattice structural parameters of a, b, γ, as shown in this figure and listed in Table 1. Each unit cell is denoted by an integer and a letter, where an integer represents the number of Au atoms per unit cell and a letter represents each distinct unit cell with the same number of Au atoms.

leading to stronger surface hydration. Finally, MD simulation studies of the adsorption process of lysozyme on the four PAM brushes showed that in contrast to the pHPenAA-induced lysozyme adsorption, three pHMAA, pHEAA, and pHPAA brushes exhibited a stronger surface resistance to lysozyme adsorption in a decreasing order of pHEAA > pHMAA >

https://dx.doi.org/10.1021/acs.langmuir.0c00165
Langmuir 2020, 36, 2757−2766

pHPAA. Our simulation results are consistent with our experimental results of the four PAM brushes, including surface wettability from contact angle and protein adsorption from surface plasmon resonance (SPR).[13] This work provides the better fundamental knowledge on a structure−property relationship among packing structure, surface hydration, and antifouling property of polymer brushes at a molecular level, which hopefully helps to design more effective antifouling materials and surfaces.

MATERIALS AND METHODS

Model Construction of PAM Brushes. In this work, we constructed four PAM brush models (pHMAA, pHEAA, pHPAA, and pHPenAA) in the presence of an explicit TIP3P water model to study surface hydration of PAM brushes. Force-field parameters of HMAA, HEAA, HPAA, and HPenAA monomers were created using the ParaChem tool[54] (https://cgenff.paramchem.org/), compatible with the CHARMM force field. Lysozyme (LYZ, PDB ID: 7LYZ)[55] was used as a model protein to study its interaction with the four PAM brushes. The CHARMM27 parameter set with the CMAP correction[56] was applied to model the lysozyme, water (TIP3P model), and ions.

Figure 1 shows the modeling process of PAM brushes in the absence and presence of lysozyme. Briefly, a single PAM chain was first created by connecting five repeated AM monomers of HMAA, HEAA, HPAA, and HPenAA to an initiator on gold and then energy minimized, where HMAA, HEAA, HPAA, and HPenAA monomers contained one, two, three, and five methylene spacer groups between the hydroxyl group and amide group, respectively (Figure 1a). An optimal single PAM chain was then built on each distinct unit cell that was periodically duplicated in a 6 × 6 array to construct a PAM brush with a specific PAM chain and unit cell. Use of a combination of four PAM chains ($HMAA_5$, $HEAA_5$, $HPAA_5$, and $HPenAA_5$), 12 chain orientation (from 0 to 360° in an increment of 30°), and 28 unit cells (Table 1 and Figure 2) enables to construct different PAM brushes with different packing structures. The geometric parameters (a, b, γ, and area) of different unit cells are listed in Table 1, where a and b are the two vector lengths of different unit cells, γ is an angle between a and b, and area is a surface area of unit cell. Therefore, for a given PAM chain, we created a 6 × 6 array of PAM chains to model the packing structure of a PAM brush by using 28 unit cells to describe different lattice structures and by rotating PAM chains from 0 to 360° by every 30° to describe different chain orientations. The optimal packing structure of PAM brushes was determined at the lowest-energy state by comparing all packing energies of different PAM brushes (Figure 1b). After optimal packing structure of the four optimal pHMAA, pHEAA, pHPAA, and pHPenAA brushes were obtained, the much larger polymer brushes (Figure 1c) were built using a 15 × 9 array (135 PAM chains) and solvated by TIP3P-modeled water molecules to better study their surface hydration in the absence of lysozyme (Figure 1d) and to study the protein resistance ability in the presence of lysozymes (Figure 1e).

Model Construction of a Protein on PAM Brushes. To study protein resistance behavior of four PAM brushes, a model protein of the lysozyme was placed on four PAM brushes in the presence of implicit or explicit water molecules and ions by using two-stage simulations to overcome the timescale limit of molecular simulations, where Monte Carlo (MC) simulations were first used to determine the optimal orientation of lysozymes on PAM brushes in the presence of implicit water molecules, and then MD simulations were performed for the adsorption or desorption process of lysozymes with optimal orientation on PAM brushes in the presence of explicit water molecules. Specifically, MC simulations were performed to determine optimal orientations of a lysozyme on PAM brushes. Based on the optimal packing structure of PAM brushes, a lysozyme was initially and randomly placed at different separation distances of 3−10 Å from the optimal PAM brushes. During 1 million step MC simulations, at a given separation distance between lysozyme and PAM brush, the center mass of the lysozyme was fixed while still allowing to freely rotate to find its optimal orientation at the lowest energy state at this separation distance. Following the same protocol, when the lysozyme was moved to different positions with its mass center being fixed, a series of optimal orientations of the lysozyme on PAM brushes were obtained and compared at different separation distances, among which the lowest-energy orientation of the lysozyme was identified and then used for subsequent MD simulations of the lysozyme adsorption process. The details of MD simulations of lysozymes on PAM brushes were described below.

MD Simulation Protocol. For each PAM brush model with or without a lysozyme, two energy minimizations were performed to remove bad contacts and relax the systems prior to MD simulations. First, 5000-step conjugate gradient minimization was performed under the position constrains on PAM chains and a lysozyme to relax water molecules; then, additional 5000-step minimization was conducted to relax all atoms only with sulfur atoms being fixed. After energy minimization, a short 0.5 ns MD simulation with a small time-step of 1 fs was performed to relax water molecules and ions with the fixed atoms of PAM chains and lysozyme, followed by additional 0.5 ns MD simulations with fixed sulfur atoms at a 1 fs time step.

For the equilibrium and production MD runs, all-atom MD simulations were conducted to simulate pure PAM brushes (pHMAA, pHEAA, pHPAA, and pHPenAA) and PAM−lysozyme systems (pHMAA−LYZ, pHEAA−LYZ, pHPAA−LYZ, and pHPenAA−LYZ) under the *NVT* ensemble (constant number of atoms, volume, and temperature) using the NAMD 2.12 program with the CHARMM force field.[56] The Langevin thermostat method with a damping coefficient of 1 ps^{-1} was used to control the temperature at 298 K. All covalent bonds involving hydrogen bonds were constrained using the RATTLE method, so that 2 fs was used to integrate the Newton motion equations using the velocity Verlet algorithm. Short-range van der Waals (vdW) interactions were calculated by the switching functions with a twin-range cutoff at 12 and 14 Å, while long-range electrostatic interactions were calculated by the particle mesh Ewald with a grad space of 0.5 Å. MD trajectories of each system were collected every 2 ps for the later analysis.

RESULTS AND DISCUSSION

Optimal Packing Structures of PAM Brushes. Packing structure of PAM brushes, as defined by chain packing density and chain orientation, is critical for accurately describing their structural-dependent surface hydration and protein resistance capacity.[57] For any given PAM chain, we constructed 6 × 6 unit cells containing a total of 36 PAM chains to model the packing structure of the PAM brush by using different unit cells (Figure 2) to describe different packing densities and by rotating PAM brush chains from 0 to 360° by every 30° to describe different chain orientations. The unit cell is defined by different Au atoms (solid cycles) and its lattice parameters (a, b, and γ area in Table 1). Unit cells that have the same Au atoms (e.g., the same surface area) may have different lattice structures (e.g., different shapes). The surface areas of the unit cells containing 4−12 Au atoms correspond to 28.8, 36.0, 43.2, 50.4, 57.6, 64.8, 72.0, 79.3, and 86.4 $Å^2$, respectively. Thus, for a given PAM brush, a total of 336 packing structures were generated, and the optimal packing structure of PAM brushes were determined by the lowest packing energies in an implicit solvent by the molecular mechanics (MM) calculation.

Figure 3 shows the packing energies of the four different pHMAA, pHEAA, pHPAA, and pHPenAA brushes as a function of 28 unit cells with optimal chain orientation being already identified from 12 orientations for the same unit cell. For all PAM brushes, there always existed an optimal unit cell to better accommodate PAM chains driven by the most favorable chain−chain interactions, that is, very small unit cells

https://dx.doi.org/10.1021/acs.langmuir.0c00165
Langmuir 2020, 36, 2757−2766

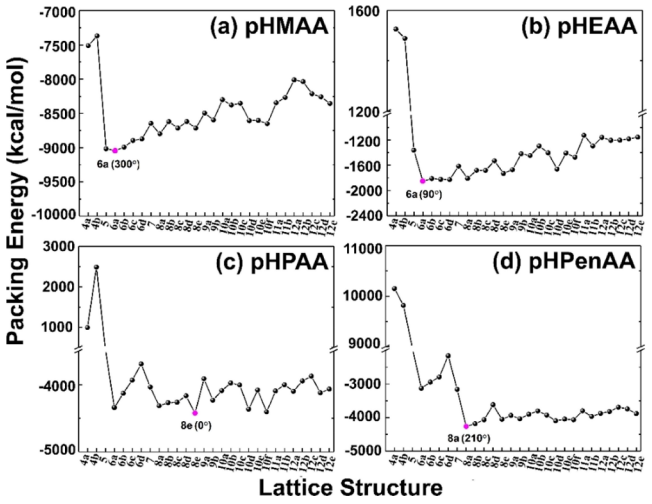

Figure 3. Searching for the optimal packing structure (rosy solid circles) of four PAM brushes. Packing energies of (a) pHMAA, (b) pHEAA, (c) pHPAA, and (d) pHPenAA brushes with an optimal chain orientation as a function of unit cells. In each unit cell, PAM chain orientation is also considered by varying from 0 to 360° with an increase of 30°.

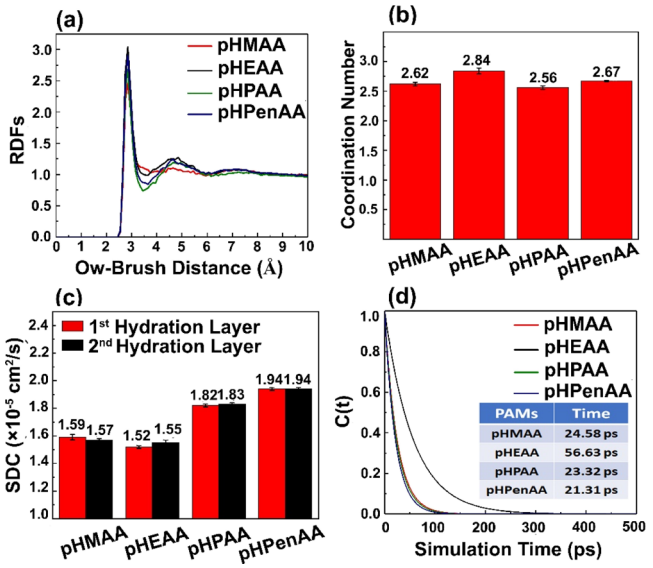

Figure 4. Structure and dynamics of water molecules on the four PAM brushes. (a) RDFs, (b) coordination number (N_w), (c) SDC, and (d) mean residence time of water molecules on pHMAA, pHEAA, pHPAA, and pHPenAA brushes.

(4a, 4b) led to the overpacking of PAM brushes because of unfavorable steric repulsion of the sidechains of PAM brushes as evidenced by much less favorable packing energies, while too large unit cells cause the loosely packed chains to twist and disorder, resulting in the reduction in vdW interactions between PAM chains. Specifically, pHMAA and pHEAA brushes with the smaller CSLs = 1, 2 reached their lowest-packing energy structure of 6a with a chain orientation of 300° and 6a with a chain orientation of 90°, respectively. Differently, because both pHPAA and pHPenAA contained the longer sidechains, they favored to adopt the larger unit cells of 8e (0°) and 8a (210°) for stretching out sidechains at the lowest-packing energy state, respectively. Taken together, for the four PAM brushes at an optimal lattice structure, the chain−chain spacing/unit cell area was 43.2 Å^2 for pHMAA, 43.2 Å^2 for pHEAA, 57.6 Å^2 for pHPAA, and 57.6 Å^2 for pHPenAA, respectively, in which polymer chains not only are flexible, but also align parallel to each other.

Water Structure and Dynamics on PAM Brushes. It is well known that the antifouling property of surfaces strongly depend on their surface hydration capacity. In this work, upon the optimal packing structures of the four PAM brushes were determined, we solvated the PAM brushes and conducted all-atom explicit-water MD simulations to study the structure and dynamics of the interfacial water layer on different PAM brushes. To illustrate the interfacial water structure, Figure 4a shows RDFs of water molecules on the four different PAM brushes. First of all, all RDFs of pHMAA, pHEAA, pHPAA, and pHPenAA brushes exhibited two obvious hydration peaks at almost the same locations of 2.85 and 4.7 Å, respectively, where the first hydration peak was much more pronounced than the second one. The RDF intensity of the first hydration peak was 2.47, 3.07, 2.79, and 2.97 for pHMAA, pHEAA, pHPAA, and pHPenAA, respectively. The higher water peak indicates the more water molecules around polymer brushes. In addition, the four polymer brushes had the higher intensity of the first water peak than the corresponding monomers in our previous work,[58] indicating that a well-packed polymer brush are more favorable to attract the surrounding water molecules than randomly distributed monomers in bulk. Beyond the first solvation shell, the second hydration layers of all brushes were much weaker, but still higher than a water bulk density of 1.0, indicating that both hydration layers interact with polymer brushes. Furthermore, the overall water intensities of pHEAA were higher than those of the other three brushes, suggesting that pHEAA brush attracts more water molecules than the other brushes. To further analyze RDF profiles, the coordination number (N_w) of water molecules around pHMAA, pHEAA, pHPAA, and pHPenAA brushes was counted by integrating the first hydration shell of RDFs from Figure 4a. It can be seen in Figure 4b that N_w on pHMAA, pHEAA, pHPAA, and pHPenAA was 2.62, 2.84, 2.56, and 2.67, respectively. The difference in N_w is another indicator that more water molecules are favorable to stay around pHMAA and pHEAA chains with the shorter CSLs = 1, 2 than pHPAA with the longer CSLs = 3.

From a dynamic viewpoint of a water hydration shell around different PAM brushes, we first evaluated the self-diffusion coefficients (SDC) of water molecules within the first and the second hydration shells of the four different PAM brushes (Figure 4c). SDC of water molecules within the first/second hydration shells of pHMAA, pHEAA, pHPAA, and pHPenAA brushes were 1.59/1.57, 1.52/1.55, 1.82/1.83, and 1.94/1.94 × 10^{-5} cm^2/s, respectively. For any given PAM brush, SDC of water molecules in the first hydration shell was almost the same as SDC in the second hydration shell. SDCs of water molecules on the four PAM brushes were much smaller than that of bulk water (2.54 × 10^{-5} cm^2/s), clearly indicating that the existence of polymer−water interactions slows down water movement at polymer−water interfaces. Furthermore, SDC of water molecules showed an increased order of pHEAA < pHMAA < pHPAA < pHPenAA, again indicating that pHMAA and pHEAA with the shorter CSLs = 1, 2 interact more favorably with interfacial water molecules than pHPAA, and pHPenAA with the longer CSLs = 3, 5 in both hydration shells.

Besides SDC, another important dynamic property of water molecules is the residence time of water molecules in the first

https://dx.doi.org/10.1021/acs.langmuir.0c00165
Langmuir 2020, 36, 2757−2766

hydration shell of PAM brushes. A longer lifetime indicates a more stable polymer−water association. The residence time is determined by fitting the function of $C_R(t) = \frac{1}{N_w}\sum_{j=1}^{N_{water}} \frac{\langle P_{Rj}(0)P_{Rj}(t)\rangle}{\langle P_{Rj}(0)^2\rangle}$ with $C_R(t) = A\ \exp(-t/\tau_s)$, where P_{Rj} is a binary function, value of 1 (0) indicates that the jth water stays (leaves) in (from) a layer with a thickness of R at a time of t. In Figure 4d, $C_R(t)$ curves for pHMAA, pHEAA, and pHPAA brushes with short CSLs decayed slower than pHPenAA with long CSL, showing a decreased order of pHEAA (56.63 ps) > pHMAA (24.58 ps) > pHPAA (23.32 ps) > pHPenAA (21.31 ps), consistent with SDC results. Different SDC and residence times indicate different interaction strengths between different brush−water contact pairs, among which more water molecules favor to form the stronger and more stable association with pHEAA brush than the other three brushes. Our previous sum frequency generation (SFG) data[13] also showed that pHMAA, pHEAA, and pHPAA brushes with the CSLs = 1, 2, and 3 exhibited similar features and peak locations in SFG spectra, while the pHPenAA brush with CSLs = 5 had a relatively lower SFG signal intensity in comparison with SFG signal intensities from the other three PAM brushes, indicating higher hydrophobicity of pHPenAA leading to its weaker ability to interact with interfacial water molecules. Further, SFG signal intensities of the "dry" PAMs brushes exhibited a decreasing order of pHEAA > pHMAA > pHPAA > pHPenAA, suggesting the ability of holding water molecules of the four PAM brushes follows the order of pHEAA > pHMAA > pHPAA > pHPenAA. Considering that the strength of surface hydration depends on the quality and quantity of water molecules interacting with PAM brushes, collective data from RDFs, coordination number, SDC, and residence time of water molecules on PAM brushes showed a CSL-dependent surface hydration behavior, that is, pHMAA and pHEAA with shorter CSLs = 1, 2 induce stronger surface hydration than pHPAA and pHPenAA with longer CSLs = 3, 5.

Surface Resistance of PAM Brushes to a Protein. To study protein adsorption (resistance) on PAM brushes, molecular simulations were performed in two steps: we first applied Metropolis MC simulations to determine the optimal orientation of a LYZ above the PAM brushes, and then performed all-atom explicit-water MD simulations to study the interactions of a protein with different PAM brushes. Upon two-million steps of MC simulations, a lysozyme adopted a similar orientation on the four PAM brushes at the corresponding lowest-energy states, that is, a V-shape region of the lysozyme was oriented away from the PAM brushes for all brushes (Figure 5).

Upon the optimal orientations of a lysozyme on different PAMs were determined, the lysozyme was manually placed at a separation distance of ∼4 Å (i.e., between the first and second hydration shells) above PAM brushes with its optimal orientation. Considering some time- and length-scale constraints from conventional MD simulations, the lysozyme was initially placed between the first and second hydration shells from PAM brushes at the pre-adsorbed state, so in this way, the less energy barrier was imposed on the lysozyme for its adsorption, and if the lysozyme is still rejected by PAM brushes, this confirms that the first hydration shell indeed produces a physical and energetic barrier to resist protein adsorption. Figure 6 shows the adsorption or desorption process of a lysozyme on the four PAM brushes during 80 ns

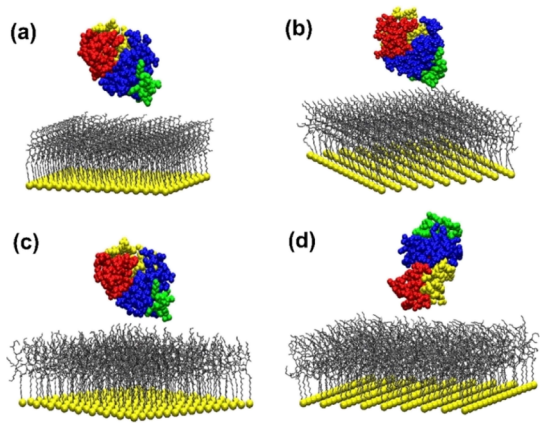

Figure 5. Optimal orientation of a lysozyme on (a) pHMAA, (b) pHEAA, (c) pHPAA, and (d) pHPenAA brushes.

MD simulations. Visual inspection of MD trajectories clearly showed that the lysozyme was desorbed from pHMAA (Figure 6a), pHEAA (Figure 6b), and pHPAA (Figure 6c), but adsorbed on pHPenAA (Figure 6d). Time-dependent separation distance profiles showed different adsorption/desorption scenarios at the atomic level details. The lysozyme quickly flied away from pHMAA and pHEAA brushes in the first 10 ns, and the desorption of the lysozyme from pHEAA brush was even more pronounced. For the pHPAA brush, the lysozyme tended to maintain weak contacts with the pHPAA brush and floated around at the brush surface, as evidenced by a short separation distance of 0−10 Å within the first 35 ns. However, after 35 ns, the lysozyme was gradually rotated and drifted away from the pHPAA brush. Thus, the lysozyme is not likely to adsorb on pHMAA, pHEAA, and pHPAA brushes. Different from the above-mentioned three brushes, the lysozyme was tightly bound to the pHPenAA brush throughout the entire 80 ns simulation. At the lysozyme−pHPenAA interface, some polar residues (Thr_{69} and Ser_{100}), negatively charged residue (Asp_{101}), and nonpolar residues (Pro_{70}, Gly_{71}, and Gly_{102}) apparently showed strong interactions with pHPenAA, as evidenced by their stable and close contacts (data not shown). This indicates that lysozyme adsorption on the pHPenAA brush is likely driven by a combination of hydrophobic interactions, hydrogen bonding, and electrostatic interactions at the interface, presumably because the increased hydrophobic property of the pHPenAA brush also reduce the surface hydration strength.

Statistically, we further analyzed the binding probability (%) of the lysozyme to the four different PAM brushes by using the separation distance profiles. We used the lysozyme−brush separation distance of <6, 6−12, and >12 Å to define the strong, weak, and no binding events of the lysozyme to PAM brushes. These binding events were counted every 1 ps and converted into binding probabilities during 80 ns MD simulations. In Figure 7, strong/weak/no binding probability (%) of the lysozyme to pHMAA, pHEAA, pHPAA, and pHPenAA brushes were 1.1%/6.0%/92.9%, 1.5%/1.1%/97.4%, 28.8%/13.1%/58.1%, and 98.5%/1.5%/0.0%, respectively. Both pHMAA and pHEAA brushes with shorter CSLs = 1, 2 had very high no binding probability of 92.9 and 97.4% to resist lysozyme adsorption. However, no-binding probability was significantly reduced to 58.1% for the pHPAA brush, indicating a weaker antifouling property. In contrast, pHPenAA had 0.0% of no binding, but 100.0% of strong

https://dx.doi.org/10.1021/acs.langmuir.0c00165
Langmuir 2020, 36, 2757−2766

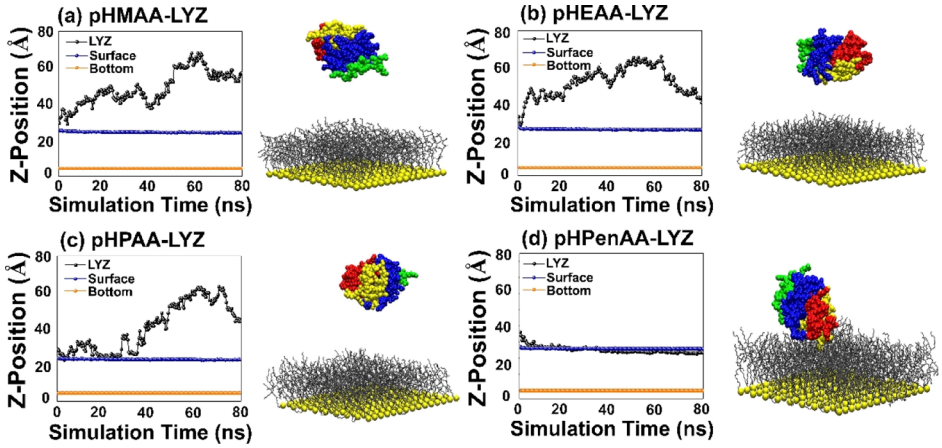

Figure 6. Time-dependent separation distance and final MD snapshots of a lysozyme with respect to (a) pHMAA, (b) pHEAA, (c) pHPAA, and (d) pHPenAA brushes.

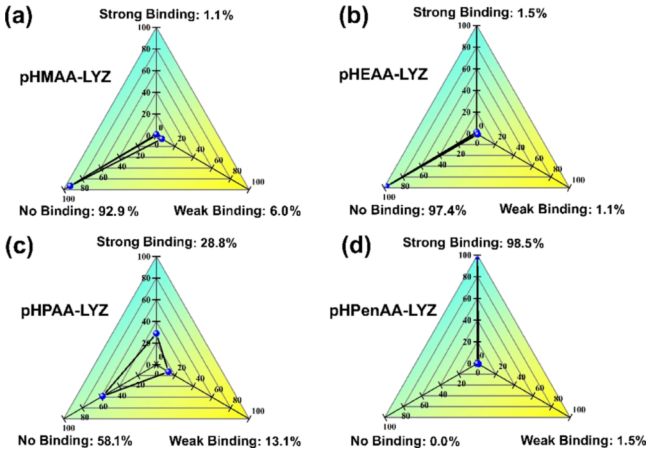

Figure 7. Binding probability (%) of a lysozyme on (a) pHMAA, (b) pHEAA, (c) pHPAA, and (d) pHPenAA brushes. Strong, weak, and no binding are defined in terms of a lysozyme−brush distance of <6, 6−12, and >12 Å, respectively.

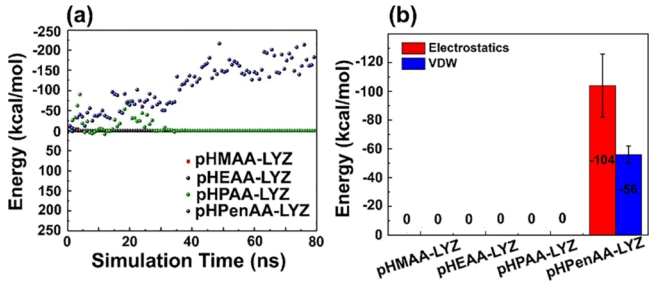

Figure 8. Intermolecular interactions between a lysozyme and PAM brushes. (a) Time-dependent nonbonded interaction energy and (b) decomposed electrostatic and vdW components between a lysozyme and the four PAM brushes (pHMAA, pHEAA, pHPAA, and pHPenAA). Data in (b) are averaged using the last 40 ns MD simulation data from (a).

binding probability to the lysozyme, suggesting its noninert property.

Comparison of different lysozyme−PAM systems reveals different adsorption/desorption behaviors of the lysozyme on PAM brushes, strongly depending on lysozyme−PAM interactions. Here, the nonbonded interaction energy between the lysozyme and PAM chains was calculated to better understand the driving forces for the adsorption/desorption of the lysozyme on PAM brushes. As shown in Figure 8a, because the lysozyme finally flied away from pHMAA, pHEAA, and pHPAA brushes, no interaction energies were observed after 35 ns for the three cases. This indicates that the lysozyme cannot break through the first hydration shell of these PAM brushes for its adsorption. In contrast, the pHPenAA brush indeed promoted the surface interaction with the lysozyme, leading to a strong surface adsorption. The averaged lysozyme−pHPenAA interaction from the last 40 ns simulations was −160 kcal/mol. Further energy decompositions (Figure 8b) showed that electrostatic and vdW interactions were −104 and −56 kcal/mol, respectively. While electrostatic interactions were ∼2 times larger than vdW interactions, occupying 65% of total nonbonded interactions, both interactions provide the collaborative and attractive forces for lysozyme adsorption.

In our previous study,[13] while all PAM brushes displayed hydrophilic character, pHMAA, pHEAA, and pHPAA brushes exhibited small contact angles of 14−18°, but the pHPenAA brush had a much larger contact angle of 52°. Surface wettability data are consistent with our collective simulation data from RDF, SDC, and residence time, both indicating different CSL-induced surface hydration strengths. As a result, further SPR results showed that pHMAA and pHEAA brushes exhibited almost undetectable protein adsorption (<0.3 ng/cm^2) from undiluted blood plasma and serum, pHPAA brushes showed a very low protein adsorption of 0.3 ng/cm^2 from the blood serum and 0.9 ng/cm^2 from the blood plasma, and pHPenAA brushes had a relatively higher protein adsorption of 0.7 ng/cm^2 from the blood serum and 2.1 ng/cm^2 from the blood plasma. Taken together, both simulation and experimental results confirm the CSLs-dependent antifouling efficiency in a decrease order of pHEAA ≥ pHMAA > pHPAA > pHPenAA. The increase in the number of methylene groups (i.e., CSL) will increase a hydrophobicity/hydrophilicity ratio of PAM chains and alter the flexibility of PAM chains, both of which would lead to different water−polymer interactions to induce different surface hydration and antifouling behaviors for different polymer brushes.

CONCLUSIONS

In this work, we computationally studied the packing structure, surface hydration, and protein resistance of the four different

https://dx.doi.org/10.1021/acs.langmuir.0c00165
Langmuir 2020, 36, 2757−2766

PAM brushes with different CSLs = 1, 2, 3, and 5 using a combination of MM, MC, and MD simulations, where MM was used to determine the optimal packing structure of PAM brushes, MC for determining the optimal orientation of a lysozyme on PAM brushes, and MD for determining the structural, dynamic, and energetic behavior between interfacial water molecules, a protein, and PAM brushes. First, because of the presence of the relatively large pendant sidechains in all PAM brushes, four PAM brushes adopted different packing structures based on different unit cells for pHMAA (a = 8.652 Å, b = 4.995 Å, γ = 90°), pHEAA (a = 8.652 Å, b = 4.995 Å, γ = 90°), pHPAA (a = 9.990 Å, b = 5.768 Å, γ = 90°), and pHPenAA (a = 11.536 Å, b = 4.995 Å, γ = 90°). Upon obtaining optimal packing structures of PAM brushes, the structural and dynamic properties of water molecules on the four PAM brushes were analyzed to determine the strength of surface hydration. Collective simulation data from RDFs, coordination number, self-diffusion, and residence time of interfacial water molecules showed that pHMAA and pHEAA with the shorter CSLs = 1−2 enabled to have a stronger and more stable interaction with more water molecules than pHPAA and pHPenAA with the longer CSLs = 3 and 5, thus creating a stronger surface hydration layer. Finally, the MD simulation of the adsorption process of a lysozyme on the four PAM brushes revealed the role of hydration in surface resistance to protein adsorption. Three pHMAA, pHEAA, and pHPAA brushes exhibited strong surface resistance to the lysozyme with a decreased antifouling capacity of pHEAA > pHMAA > pHPAA, in sharp contrast to a pHPenAA-induced adsorption of the lysozyme. Simulation results are consistent with our experimental results from surface wettability of the four PAM brushes by contact angles, protein adsorption on the four PAM brushes by SPR, and water binding ability to the four PAM brushes by SFG. This work provides the incremental knowledge on the CSL-dependent surface hydration and protein resistance capacity of different PAM brushes, which would help to better understand antifouling behaviors and design more effective antifouling materials and surfaces.

■ ASSOCIATED CONTENT

Supporting Information

The Supporting Information is available free of charge at https://pubs.acs.org/doi/10.1021/acs.langmuir.0c00165.

Force-field parameters of four different PAMs (PDF)

Adsorption/desorption process on pHEAA (MPG)

Adsorption/desorption process on pHMAA (MPG)

Adsorption/desorption process on pHPAA (MPG)

Adsorption/desorption process on pHPenAA (MPG)

■ AUTHOR INFORMATION

Corresponding Author

Jie Zheng − *Department of Chemical, Biomolecular, and Corrosion Engineering and Department of Polymer Engineering, The University of Akron, Akron, Ohio 44325, United States;* orcid.org/0000-0003-1547-3612; Email: zhengj@uakron.edu

Authors

Yonglan Liu − *Department of Chemical, Biomolecular, and Corrosion Engineering, The University of Akron, Akron, Ohio 44325, United States*

Dong Zhang − *Department of Chemical, Biomolecular, and Corrosion Engineering, The University of Akron, Akron, Ohio 44325, United States*

Baiping Ren − *Department of Chemical, Biomolecular, and Corrosion Engineering, The University of Akron, Akron, Ohio 44325, United States*

Xiong Gong − *Department of Polymer Engineering, The University of Akron, Akron, Ohio 44325, United States;* orcid.org/0000-0001-6525-3824

Aristo Liu − *Copley High School, Akron, Ohio 44321, United States*

Yung Chang − *Department of Chemical Engineering and R&D Center for Membrane Technology, Chung Yuan Christian University, Taoyuan 320, Taiwan;* orcid.org/0000-0003-1419-4478

Yi He − *College of Chemical and Biological Engineering, Zhejiang University, Hangzhou, Zhejiang 310027, China*

Complete contact information is available at: https://pubs.acs.org/10.1021/acs.langmuir.0c00165

Author Contributions

#Y.L. and D.Z. contribute equally to this work.

Notes

The authors declare no competing financial interest.

■ ACKNOWLEDGMENTS

This work is supported by NSF grants (DMR-1806138 and CMMI-1825122).

■ REFERENCES

(1) Chen, H.; Zhao, C.; Zhang, M.; Chen, Q.; Ma, J.; Zheng, J. Molecular Understanding and Structural-Based Design of Polyacrylamides and Polyacrylates as Antifouling Materials. *Langmuir* **2016**, *32*, 3315−3330.

(2) Meyers, S. R.; Grinstaff, M. W. Biocompatible and Bioactive Surface Modifications for Prolonged In Vivo Efficacy. *Chem. Rev.* **2012**, *112*, 1615−1632.

(3) Wei, Q.; Becherer, T.; Angioletti-Uberti, S.; Dzubiella, J.; Wischke, C.; Neffe, A. T.; Lendlein, A.; Ballauff, M.; Haag, R. Protein Interactions with Polymer Coatings and Biomaterials. *Angew. Chem., Int. Ed.* **2014**, *53*, 8004−8031.

(4) Wang, G.; Su, X.; Xu, Q.; Xu, G.; Lin, J.; Luo, X. Antifouling aptasensor for the detection of adenosine triphosphate in biological media based on mixed self-assembled aptamer and zwitterionic peptide. *Biosens. Bioelectron.* **2018**, *101*, 129−134.

(5) Mueller, J.; Davis, R. H. Protein fouling of surface-modified polymeric microfiltration membranes. *J. Membr. Sci.* **1996**, *116*, 47−60.

(6) Asuri, P.; Karajanagi, S. S.; Kane, R. S.; Dordick, J. S. Polymer-nanotube-enzyme composites as active antifouling films. *Small* **2007**, *3*, 50−53.

(7) Lin, J.; Chen, X.; Chen, C.; Hu, J.; Zhou, C.; Cai, X.; Wang, W.; Zheng, C.; Zhang, P.; Cheng, J.; Guo, Z.; Liu, H. Durably Antibacterial and Bacterially Antiadhesive Cotton Fabrics Coated by Cationic Fluorinated Polymers. *ACS Appl. Mater. Interfaces* **2018**, *10*, 6124−6136.

(8) Hu, J.; Lin, J.; Zhang, Y.; Lin, Z.; Qiao, Z.; Liu, Z.; Yang, W.; Liu, X.; Dong, M.; Guo, Z. A new anti-biofilm strategy of enabling arbitrary surfaces of materials and devices with robust bacterial anti-adhesion via a spraying modified microsphere method. *J. Mater. Chem. A* **2019**, *7*, 26039−26052.

(9) Hao, X.; Chen, S.; Qin, D.; Zhang, M.; Li, W.; Fan, J.; Wang, C.; Dong, M.; Zhang, J.; Cheng, F.; Guo, Z. Antifouling and antibacterial behaviors of capsaicin-based pH responsive smart coatings in marine environments. *Mater. Sci. Eng., C* **2020**, *108*, 110361.

(10) Nautiyal, A.; Qiao, M.; Ren, T.; Huang, T.-S.; Zhang, X.; Cook, J.; Bozack, M. J.; Farag, R. High-performance Engineered Conducting Polymer Film towards Antimicrobial/Anticorrosion Applications. *Eng. Sci.* **2018**, *4*, 70−78.
(11) Shah, N.; Aslam, S.; Islam, M.; Arain, M.; Rehan, T.; Naeem, M.; Ullah, M.; Yang, G. Fabrication of thermally stable graphite-based poly(acrylonitrile-co-acrylic acid) composite with impressive antimicrobial properties. *Eng. Sci.* **2019**, *6*, 77−85.
(12) Zheng, J.; He, Y.; Chen, S.; Li, L.; Bernards, M. T.; Jiang, S. Molecular simulation studies of the structure of phosphorylcholine self-assembled monolayers. *J. Chem. Phys.* **2006**, *125*, 174714.
(13) Yang, J.; Zhang, M.; Chen, H.; Chang, Y.; Chen, Z.; Zheng, J. Probing the Structural Dependence of Carbon Space Lengths of Poly(N-hydroxyalkyl acrylamide)-Based Brushes on Antifouling Performance. *Biomacromolecules* **2014**, *15*, 2982−2991.
(14) Liu, Q.; Singh, A.; Lalani, R.; Liu, L. Ultralow fouling polyacrylamide on gold surfaces via surface-initiated atom transfer radical polymerization. *Biomacromolecules* **2012**, *13*, 1086−1092.
(15) Bauer, S.; Arpa-Sancet, M. P.; Finlay, J. A.; Callow, M. E.; Callow, J. A.; Rosenhahn, A. Adhesion of Marine Fouling Organisms on Hydrophilic and Amphiphilic Polysaccharides. *Langmuir* **2013**, *29*, 4039−4047.
(16) Luxenhofer, R.; Fetsch, C.; Grossmann, A. Polypeptoids: A perfect match for molecular definition and macromolecular engineering? *J. Polym. Sci., Part A: Polym. Chem.* **2013**, *51*, 2731−2752.
(17) Sohn, E.-H.; Ahn, J.; Bhang, S. H.; Kang, J.; Yoon, J.; Kim, B.-S.; Lee, J.-C. Bacterial adhesion-resistant poly(2-hydroxyethyl methacrylate) derivative for mammalian cell cultures. *Macromol. Biosci.* **2012**, *12*, 211−217.
(18) Yang, F.; Liu, Y.; Zhang, Y.; Ren, B.; Xu, J.; Zheng, J. Synthesis and Characterization of Ultralow Fouling Poly(N-acryloyl-glycinamide) Brushes. *Langmuir* **2017**, *33*, 13964−13972.
(19) Liu, C.; Faria, A. F.; Ma, J.; Elimelech, M. Mitigation of Biofilm Development on Thin-Film Composite Membranes Functionalized with Zwitterionic Polymers and Silver Nanoparticles. *Environ. Sci. Technol.* **2017**, *51*, 182−191.
(20) Zhang, Z.; Chen, S.; Chang, Y.; Jiang, S. Surface grafted sulfobetaine polymers via atom transfer radical polymerization as superlow fouling coatings. *J. Phys. Chem. B* **2006**, *110*, 10799−10804.
(21) Yu, B.-Y.; Zheng, J.; Chang, Y.; Sin, M.-C.; Chang, C.-H.; Higuchi, A.; Sun, Y.-M. Surface Zwitterionization of Titanium for a General Bio-Inert Control of Plasma Proteins, Blood Cells, Tissue Cells, and Bacteria. *Langmuir* **2014**, *30*, 7502−7512.
(22) Wu, J.; Zhao, C.; Hu, R.; Lin, W.; Wang, Q.; Zhao, J.; Bilinovich, S. M.; Leeper, T. C.; Li, L.; Cheung, H. M.; Chen, S.; Zheng, J. Probing the weak interaction of proteins with neutral and zwitterionic antifouling polymers. *Acta Biomater.* **2014**, *10*, 751−760.
(23) Zhao, C.; Zhao, J.; Li, X.; Wu, J.; Chen, S.; Chen, Q.; Wang, Q.; Gong, X.; Li, L.; Zheng, J. Probing structure-antifouling activity relationships of polyacrylamides and polyacrylates. *Biomaterials* **2013**, *34*, 4714−4724.
(24) Zhang, Z.; Zhang, M.; Chen, S.; Horbett, T. A.; Ratner, B. D.; Jiang, S. Blood compatibility of surfaces with superlow protein adsorption. *Biomaterials* **2008**, *29*, 4285−4291.
(25) Zhang, Z.; Chen, S.; Jiang, S. Dual-functional biomimetic materials: Nonfouling poly(carboxybetaine) with active functional groups for protein immobilization. *Biomacromolecules* **2006**, *7*, 3311−3315.
(26) Brynda, E.; Surman, F.; Rodriguez-Emmennegger, C.; Riedel, T.; Vaisocherova, H. L. New Copolymer Brushes for Label-Free Affinity Biosensors. *IEEE Sens.* **2015**, 1626−1629.
(27) Yang, W.; Xue, H.; Li, W.; Zhang, J.; Jiang, S. Pursuing "Zero" Protein Adsorption of Poly(carboxybetaine) from Undiluted Blood Serum and Plasma. *Langmuir* **2009**, *25*, 11911−11916.
(28) Chen, H.; Yang, J.; Xiao, S.; Hu, R.; Bhaway, S. M.; Vogt, B. D.; Zhang, M.; Chen, Q.; Ma, J.; Chang, Y.; Li, L.; Zheng, J. Salt-responsive polyzwitterionic materials for surface regeneration between switchable fouling and antifouling properties. *Acta Biomater.* **2016**, *40*, 62−69.
(29) Yang, J.; Chen, H.; Xiao, S.; Shen, M.; Chen, F.; Fan, P.; Zhong, M.; Zheng, J. Salt-Responsive Zwitterionic Polymer Brushes with Tunable Friction and Antifouling Properties. *Langmuir* **2015**, *31*, 9125−9133.
(30) Prime, K. L.; Whitesides, G. M. Adsorption of proteins onto surfaces containing end-attached oligo(ethylene oxide): a model system using self-assembled monolayers. *J. Am. Chem. Soc.* **1993**, *115*, 10714−10721.
(31) Li, L.; Chen, S.; Zheng, J.; Ratner, B. D.; Jiang, S. Protein Adsorption on Oligo(ethylene glycol)-Terminated Alkanethiolate Self-Assembled Monolayers: The Molecular Basis for Nonfouling Behavior. *J. Phys. Chem. B* **2005**, *109*, 2934−2941.
(32) Collinson, M.; Bowden, E. F.; Tarlov, M. J. Voltammetry of Covalently Immobilized Cytochrome-C on Self-Assembled Monolayer Electrodes. *Langmuir* **1992**, *8*, 1247−1250.
(33) Chen, S.; Liu, L.; Jiang, S. Strong resistance of oligo-(phosphorylcholine) self-assembled monolayers to protein adsorption. *Langmuir* **2006**, *22*, 2418−2421.
(34) Chen, S.; Zheng, J.; Li, L.; Jiang, S. Strong resistance of phosphorylcholine self-assembled monolayers to protein adsorption: Insights into nonfouling properties of zwitterionic materials. *J. Am. Chem. Soc.* **2005**, *127*, 14473−14478.
(35) Ostuni, E.; Chapman, R. G.; Holmlin, R. E.; Takayama, S.; Whitesides, G. M. A Survey of Structure−Property Relationships of Surfaces that Resist the Adsorption of Protein. *Langmuir* **2001**, *17*, 5605−5620.
(36) Feldman, K.; Hähner, G.; Spencer, N. D.; Harder, P.; Grunze, M. Probing resistance to protein adsorption of oligo(ethylene glycol)-terminated self-assembled monolayers by scanning force microscopy. *J. Am. Chem. Soc.* **1999**, *121*, 10134−10141.
(37) Pertsin, A. J.; Grunze, M. Computer simulation of water near the surface of oligo(ethylene glycol)-terminated alkanethiol self-assembled monolayers. *Langmuir* **2000**, *16*, 8829−8841.
(38) Pertsin, A. J.; Hayashi, T.; Grunze, M. Grand canonical Monte Carlo Simulations of the hydration interaction between oligo(ethylene glycol)-terminated alkanethiol self-assembled monolayers. *J. Phys. Chem. B* **2002**, *106*, 12274−12281.
(39) Luk, Y.-Y.; Kato, M.; Mrksich, M. Self-assembled monolayers of alkanethiolates presenting mannitol groups are inert to protein adsorption and cell attachment. *Langmuir* **2000**, *16*, 9604−9608.
(40) Zheng, J.; Li, L.; Chen, S.; Jiang, S. Molecular simulation study of water interactions with oligo (ethylene glycol)-terminated alkanethiol self-assembled monolayers. *Langmuir* **2004**, *20*, 8931−8938.
(41) Zheng, J.; Li, L.; Tsao, H.-K.; Sheng, Y.-J.; Chen, S.; Jiang, S. Strong Repulsive Forces between Protein and Oligo (Ethylene Glycol) Self-Assembled Monolayers: A Molecular Simulation Study. *Biophys. J.* **2005**, *89*, 158−166.
(42) Prime, K.; Whitesides, G. Self-assembled organic monolayers: model systems for studying adsorption of proteins at surfaces. *Science* **1991**, *252*, 1164−1167.
(43) Zhang, Z.; Vaisocherová, H.; Cheng, G.; Yang, W.; Xue, H.; Jiang, S. Nonfouling Behavior of Polycarboxybetaine-Grafted Surfaces: Structural and Environmental Effects. *Biomacromolecules* **2008**, *9*, 2686−2692.
(44) Zhou, J.; Zheng, J.; Jiang, S. Molecular simulation studies of the orientation and conformation of cytochrome c adsorbed on self-assembled monolayers. *J. Phys. Chem. B* **2004**, *108*, 17418−17424.
(45) He, Y.; Hower, J.; Chen, S.; Bernards, M. T.; Chang, Y.; Jiang, S. Molecular simulation studies of protein interactions with zwitterionic phosphorylcholine self-assembled monolayers in the presence of water. *Langmuir* **2008**, *24*, 10358−10364.
(46) Liu, J.; Zhou, J. Hydrolysis-controlled protein adsorption and antifouling behaviors of mixed charged self-assembled monolayer: A molecular simulation study. *Acta Biomater.* **2016**, *40*, 23−30.
(47) Cheung, D. L.; Lau, K. H. A. Atomistic Study of Zwitterionic Peptoid Antifouling Brushes. *Langmuir* **2019**, *35*, 1483−1494.
(48) Penna, M.; Ley, K. J.; Belessiotis-Richards, A.; MacLaughlin, S.; Winkler, D. A.; Yarovsky, I. Hydration and Dynamics of Ligands

https://dx.doi.org/10.1021/acs.langmuir.0c00165
Langmuir 2020, 36, 2757−2766

Determine the Antifouling Capacity of Functionalized Surfaces. *J. Phys. Chem. C* **2019**, *123*, 30360−30372.
(49) Unsworth, L. D.; Sheardown, H.; Brash, J. L. Protein-Resistant Poly(ethylene oxide)-Grafted Surfaces: Chain Density-Dependent Multiple Mechanisms of Action. *Langmuir* **2008**, *24*, 1924−1929.
(50) Abraham, S.; So, A.; Unsworth, L. D. Poly(carboxybetaine methacrylamide)-modified nanoparticles: A model system for studying the effect of chain chemistry on film properties, adsorbed protein conformation, and clot formation kinetics. *Biomacromolecules* **2011**, *12*, 3567−3580.
(51) Liu, Z.-Y.; Jiang, Q.; Jin, Z.; Sun, Z.; Ma, W.; Wang, Y. Understanding the Antifouling Mechanism of Zwitterionic Monomer-Grafted Polyvinylidene Difluoride Membranes: A Comparative Experimental and Molecular Dynamics Simulation Study. *ACS Appl. Mater. Interfaces* **2019**, *11*, 14408−14417.
(52) Xiang, Y.; Xu, R.-G.; Leng, Y. Molecular Dynamics Simulations of a Poly(ethylene glycol)-Grafted Polyamide Membrane and Its Interaction with a Calcium Alginate Gel. *Langmuir* **2016**, *32*, 4424−4433.
(53) Xiang, Y.; Xu, R.-G.; Leng, Y. Molecular Simulations of the Hydration Behavior of a Zwitterion Brush Array and Its Antifouling Property in an Aqueous Environment. *Langmuir* **2018**, *34*, 2245−2257.
(54) Vanommeslaeghe, K.; Hatcher, E.; Acharya, C.; Kundu, S.; Zhong, S.; Shim, J.; Darian, E.; Guvench, O.; Lopes, P.; Vorobyov, I.; Mackerell, A. D., Jr. CHARMM general force field: A force field for drug-like molecules compatible with the CHARMM all-atom additive biological force fields. *J. Comput. Chem.* **2010**, *31*, 671−690.
(55) Herzberg, O.; Sussman, J. L. Protein Model-Building by the Use of a Constrained-Restrained Least-Squares Procedure. *J. Appl. Crystallogr.* **1983**, *16*, 144−150.
(56) Phillips, J. C.; Braun, R.; Wang, W.; Gumbart, J.; Tajkhorshid, E.; Villa, E.; Chipot, C.; Skeel, R. D.; Kalé, L.; Schulten, K. Scalable molecular dynamics with NAMD. *J. Comput. Chem.* **2005**, *26*, 1781−1802.
(57) Herrwerth, S.; Eck, W.; Reinhardt, S.; Grunze, M. Factors that Determine the Protein Resistance of Oligoether Self-Assembled Monolayers − Internal Hydrophilicity, Terminal Hydrophilicity, and Lateral Packing Density. *J. Am. Chem. Soc.* **2003**, *125*, 9359−9366.
(58) Liu, Y.; Zhang, Y.; Ren, B.; Sun, Y.; He, Y.; Cheng, F.; Xu, J.; Zheng, J. Molecular Dynamics Simulation of the Effect of Carbon Space Lengths on the Antifouling Properties of Hydroxyalkyl Acrylamides. *Langmuir* **2019**, *35*, 3576−3584.

https://dx.doi.org/10.1021/acs.langmuir.0c00165
Langmuir 2020, 36, 2757−2766